4

Chapter 4

Reactive Solute Diffusion in Elastico-Viscous Boundary Layer Fluid Flow over a Flat Permeable Plate with Variable Surface Concentration

4.1 Introduction

The steady fluid motion of viscous liquid past a flat surface attracts researchers because of its enormous technological applications. The study of such a type of flow was firstly initiated by Blasius [65]. Abu-Sitta [66] revealed the the existence of solution of fluid motion passing through a flat surface. Later stage, many scholars [67-68] investigated various elements of boundary layer flow across a flat surface.

The elastico-viscous fluid, which has both elastic and viscous properties, has many applications in engineering sciences. As high-velocity pressure is applied to it, it hardens and transforms from a liquid to a solid. That's why, it is now frequently used in protective equipment such as liquid body armor, liquid sports shoes, helmets, mobile cases, speed bumps, and other similar products. Hayat *et al*. [69] examined the mixed convective heat transition taking visco-elastic liquid through a stretching cylinder. Rashidi *et al.* [70]

investigated hydromagnetic mixed convective visco-elastic fluid motion taking thermal radiation.

The investigation of solute transport in fluid flow is critical for the progress of separation method and the theory of chemical kinetics. Many researchers [71-75] examined the impact of chemical processes on fluid as a result of stretching and contracting of sheets. Heat transition and mass transport in a hydromagnetic chemically reactive fluid across a flat permeable plate were demonstrated by Ibrahim and Makinde [76]. Bhattacharyya and Uddin [77] examined the chemically reactive diffusion of solute through a flat permeable plate surrounded by porous medium having variable surface concentration. Eldabe *et al.* [78] investigated the chemically reactive mass transport taking variable wall concentration for a moving flat permeable plate. The mass diffusion due to chemical reaction over an expanded exponentially surface having variable wall concentration was demonstrated by Banerjee *et al.* [79].

The mass transport and heat transition mechanism through porous media has piqued the curiosity of many scholars due to its widespread use in the chemical industry, petroleum engineering, and a range of other technological operations. Furthermore, a better understanding of convection through porous media could aid in the design of insulation, grain storage, metal processing, filtration systems, catalytic reactors, heat exchangers, and other fields. Nayak *et al*. [80] illustrated how heat and mass transmission take place via a boundary layer in a chemically reactive, hydromagnetic, viscous liquid with a source/sink. Sing and Kumar [81] investigated impact of chemical reaction on heat and mass transfer process for micropolar fluid past a porous channel using radiation. Mjankwi *et al.* [82] looked at how the heat flow and mass absorption coefficient were affected by different fluid properties. Misra and Govardhan [83] studied how heat and mass transmission process affected the boundary layer for nanofluid flow. Jabeen *et al.* [84] provided a comparative study with thermal radiation and thermophoresis with chemically reactive MHD flow along a porous stretching surface.

This paper deals with the solute diffusion resulting from chemical reaction in Elastico-viscous fluid through a flat permeable plate represented by Walter Liquid (Model B/) with variation in surface concentration. The variable reaction rate is considered in this study. Employing similarity variables, the resultant equations converted to self-similar forms and thus solved by the well-known MATLAB inbuilt solver ‘bvp4c’. For relevant flow feature

parameters, the numerically calculated results are displayed. The results of the numerical calculations are plotted for the involved flow feature values. From a physical standpoint, the fluid flow and solute transport mechanisms are thoroughly examined.

4.2 Mathematical Formulation

The diffusion of solute results from chemical reaction in Elastico-viscous fluid across a flat permeable plate surrounded by a porous domain taking variation in concentration at the plate is considered as $C_W = C_\infty + C_0 x^n$, where C_W: plate concentration, C_∞: free stream concentration, C_0: real constant, n: power-law exponent. The free stream velocity u_∞ and the concentration C_∞ away from boundary layer make up the external flow. The plate along x-axis serves a reference frame and y-axis is at right angle to it. Fig. 4.1 depicts the physical geometry of flow problem.

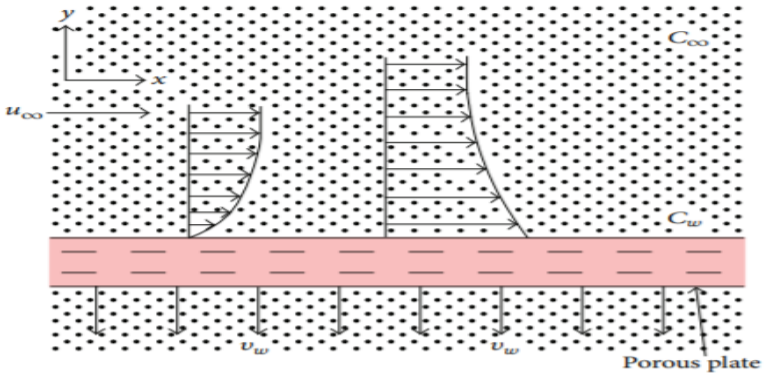

Fig. 4.1 Physical model of flow problem

The fluid motion is guided by:

$$\frac{\partial \mathrm{u}}{\partial \mathrm{x}} + \frac{\partial \mathrm{v}}{\partial \mathrm{y}} = 0 \tag{4.2.1}$$

$$\mathrm{u}\frac{\partial \mathrm{u}}{\partial \mathrm{x}} + \mathrm{v}\frac{\partial \mathrm{u}}{\partial \mathrm{y}} = \nu\frac{\partial^2 \mathrm{u}}{\partial \mathrm{y}^2} - \frac{\mathrm{k}_0}{\rho}\left[\mathrm{u}\frac{\partial^3 \mathrm{u}}{\partial \mathrm{x}\partial \mathrm{y}^2} + \mathrm{v}\frac{\partial^3 \mathrm{y}}{\partial \mathrm{y}^3} - \frac{\partial \mathrm{u}}{\partial \mathrm{y}}\frac{\partial^2 \mathrm{u}}{\partial \mathrm{x}\partial \mathrm{y}} - \frac{\partial \mathrm{v}}{\partial \mathrm{y}}\frac{\partial^2 \mathrm{u}}{\partial \mathrm{y}^2}\right] - \frac{\nu}{\mathrm{k}}(u - U_\infty) \tag{4.2.2}$$

$$\mathrm{u}\frac{\partial \mathrm{C}}{\partial \mathrm{x}} + \mathrm{v}\frac{\partial \mathrm{C}}{\partial \mathrm{y}} = D\frac{\partial^2 \mathrm{C}}{\partial \mathrm{y}^2} - \mathrm{R}(\mathrm{C} - C_\infty) \tag{4.2.3}$$

where,

u: velocity along x-axis, v: velocity along y-axis, k_0: elastico-viscous factor,

k: permeability parameter, μ: coefficient of fluid viscosity, C: concentration,

ρ: fluid density, D: diffusion coefficient, $\nu = \frac{\mu}{\rho}$: kinematic viscosity, $R(x) = \frac{LR_0}{x}$: variable reaction rate, L: reference length, R_0: constant.

The relevant conditions at the boundary are:

$$\text{At } y = 0: u = 0,\ v = v_w \text{ and as } y \to \infty: u \to u_\infty \tag{4.2.4}$$

$$\text{At } y = 0: C = C_W = C_\infty + C_0 x^n \text{ and as } y \to \infty: C \to C_\infty \tag{4.2.5}$$

where $v_w = \frac{v_0}{(x)^{\frac{1}{2}}}$: applied suction or blowing parameter for flat plate, v_0: constant also $v_0 < 0$ represents suction, and $v_0 > 0$ indicates blowing.

Stream function $\Psi(x, y)$ is connected with velocity components as

$$u = \frac{\partial \Psi}{\partial y}, v = -\frac{\partial \Psi}{\partial x} \tag{4.2.6}$$

Now, applying (4.2.6), (4.2.2) and (4.2.3) transformed as

$$\frac{\partial \Psi}{\partial y}\frac{\partial^2 \Psi}{\partial x \partial y} - \frac{\partial \Psi}{\partial x}\frac{\partial^2 \Psi}{\partial y^2} = \nu \frac{\partial^3 \Psi}{\partial y^3} - \frac{k_0}{\rho}\left[\frac{\partial \Psi}{\partial y}\frac{\partial^4 \Psi}{\partial x \partial y^3} - \frac{\partial \Psi}{\partial x}\frac{\partial^4 \Psi}{\partial y^4} - \frac{\partial^2 \Psi}{\partial y^2}\frac{\partial^3 \Psi}{\partial x \partial y^2} + \frac{\partial^2 \Psi}{\partial x \partial y}\frac{\partial^3 \Psi}{\partial y^3}\right] + \frac{\nu}{k}\left(\frac{\partial \Psi}{\partial y} - u_\infty\right) \tag{4.2.7}$$

$$\frac{\partial \Psi}{\partial y}\frac{\partial C}{\partial x} - \frac{\partial \Psi}{\partial x}\frac{\partial C}{\partial y} = D\frac{\partial^2 C}{\partial y^2} - \frac{LR_0}{x}(C - C_\infty) \tag{4.2.8}$$

Relevant boundary conditions (4.2.4) turn into:

$$\text{At } y = 0;\ \frac{\partial \Psi}{\partial y} = 0, \frac{\partial \Psi}{\partial x} = -v_w \text{ and as } y \to \infty: \frac{\partial \Psi}{\partial y} \to u_\infty \tag{4.2.9}$$

Variables without dimension, Ψ and C are taken as :

$$\Psi = \sqrt{U_\infty \nu x}\, f(\eta)\ ,\ C = C_\infty + (C_w - C_\infty)\phi(\eta) \tag{4.2.10}$$

where, $\eta = \left(\frac{y}{x}\right)\sqrt{Re_x}$: similarity variable, $Re_x = \frac{u_\infty x}{\nu}$: local Reynolds number.

Employing (4.2.10), obtain final self-similar equations as:

$$f'''(\eta)+\frac{1}{2}f(\eta)f''(\eta)+k_1\left[2f'(\eta)f'''(\eta)+f(\eta)f^{\text{iv}}(\eta)-\left(f''(\eta)\right)^2\right]-\frac{1}{Da_xRe_x}(f'(\eta)-1)=0 \quad (4.2.11)$$

$$\phi''(\eta)+\frac{1}{2}S_cf(\eta)\phi'(\eta)-S_c(nf'(\eta)+\beta)\phi(\eta)=0 \quad (4.2.12)$$

where, $Da_x=\frac{k}{x^2}=\frac{k_0}{x}$: local Darcy number, k =k_0x , k_0 being constant, k_1: modified elastic-viscous parameter, $S_c=\frac{\nu}{D}$: Schmidt number, $\beta=\frac{LR_0}{u_\infty}$: chemical reaction rate parameter having cases (i) destructive type if $\beta>0$ (ii) constructive type if $\beta<0$, and (iii) non-reactive solute

if $\beta=0$.

Equation (4.2.11) can be written as

$$f'''(\eta)+\frac{1}{2}f(\eta)f''(\eta)+k_1\left[2f'(\eta)f'''(\eta)+f(\eta)f^{\text{iv}}(\eta)-\left(f''(\eta)\right)^2\right]+k^*\left(1-f'(\eta)\right)=0 \quad (4.2.13)$$

where $k^*=\frac{1}{Da_xRe_x}$: permeability parameter.

Equations (4.2.9) and (4.2.5) are transformed as:

$$At\ \eta=0\ ;\ f(\eta)=S,\ f'(\eta)=0\ and\ as\ \eta\to\infty:\ f'(\eta)=1,\ f''(\eta)=0 \quad (4.2.14)$$

$$At\ \eta=0\ ;\phi(\eta)=1 \text{ and as } \eta\to\infty:\ \phi(\eta)=0 \quad (4.2.15)$$

where, $S=\left(\frac{-2v_w}{u_\infty}\right)(Re_x)^{\frac{1}{2}}=\frac{-2v_0}{(u_\infty\nu)^{\frac{1}{2}}}$: suction or blowing parameter having cases (i) for suction, $S>0$ when $v_0<0$ and (ii) for blowing, $S<0$ when $v_0>0$.

4.3 Method of Solution

The implement 'bvp4c' MATLAB solver to equations (4.2.13) and (4.2.12), the following transformation is adopted:

$$f=f_1,\ f'=f_2,\ f''=f_3,\ f'''=f_4\ ,\phi=f_5,\ \phi'=f_6 \quad (4.3.1)$$

Making use of (4.3.1), equations (4.2.13) and (4.2.12) can be written as:

$$f_4' = \frac{1}{f_1}\left[(f_3)^2 - 2f_2f_4 - \left(\frac{1}{k_1}\right)\left\{f_4 + \frac{1}{2}f_1f_3 + k^*(1-f_2)\right\}\right] \quad (4.3.2)$$

$$f_6' = -\frac{1}{2}S_cf_1f_6 + S_c(nf_2 + \beta)f_5 \quad (4.3.3)$$

and the applicable boundary conditions (5.2.14) and (5.2.15) reduces as follows:

$$f_1(0) = \text{S},\ f_2(0) = 0\ and\ f_2(\infty) = 1,\ f_3(\infty) = 0 \quad (4.3.4)$$

$$f_5(0) = 1\ and\ f_5(\infty) = 0 \quad (4.3.5)$$

4.4 Results and Discussion

To emphasize the physical relevance of the pertinent flow parameters, the velocity profile and concentration profile, both of which were calculated numerically, are shown in Figs. 4.2 to 4.18 using different parameter combinations like elatico-viscous k_1, permeability k*, suction/blowing S, Schmidt number S_c, first order chemical reaction rate β under direct and inverse variation.

The skin friction coefficient is assessed to judge the correctness of the numerical output produced by 'bvp4c' and to verify the current work without taking elastico-viscous and permeability parameters and is obtained as $f''(0) = 0.3321$ which is well in accord with the standard results obtained by Bhattacharyya and Layek [75] as $f''(0) = 0.332058$, Ishak, Nazir and Pop [72] $f''(0) = 0.3321$, Eldabe, Sedki and Youssef [78] $f''(0) = 0.332057$.

The velocity curves $f'(\eta)$ versus η for the various values of elastico-viscous (k_1) and permeability (k*) parameters are depicted in figures 4.2 & 4.3. The rise in k_1 and k^*, enhances the velocity profile $f'(\eta)$ at some fixed η. This indicates a reduction in the thickness of the momentum boundary layer.

The impact of suction and blowing factors on the velocity curves $f'(\eta)$ are demonstrated from figs. 4.4 and 4.5. It is noticed that growing applied suction velocity reduces and gradually settled down after traversing a certain distance. On the other hand, velocity enhances rapidly with applied blowing and settles down soon. Furthermore, the solute boundary barrier is thinner after being subjected to fluid suction, whereas blowing thickens it.

Figs. 4.6 and 4.7 depict the fluid concentration profile $\phi(\eta)$ against η with the growth of elastico-viscous parameter k_1 for direct variation and inverse variation. The concentration of the fluid for direct variation diminishes with growing elastico-viscocity but for inverse variation, though it enhances initially but gradually it diminishes and finally settles down at η = 6.

The influence of permeability factor on the concentration distribution $\phi(\eta)$ against η for direct and inverse variation are illustrated in figs. 4.8 and 4.9. Due to concentration overshoot, solute transport from the surface to the fluid occurs in direct fluctuation, whereas solute absorption at the surface occurs in inverse variation. Fig. 4.8 shows that the concentration of the fluid reduces with the rise of permeability factor for direct variation but for the inverse variation the fluid concentration diminishes initially but gradually it rises with the growing permeability factor as noticed from fig. 4.9.

The effect of applied suction for direct and inverse variation on $\phi(\eta)$, the concentration distribution, are demonstrated from figs. 4.10 and 4.11. The concentration profile reduces but not significantly as the applied suction values enhance for direct variation but for inverse variation notable reduction in concentration profile is noticed with the rise of applied suction. Thus, the thickness of solute boundary layer is diminished upon application of suction.

The impact of Schmidt number S_c on the concentration curves $\phi(\eta)$ against η for direct and inverse variation are plotted in figs. 4.12 and 4.13. The rapid reduction of concentration profile is observed from fig. 4.12 for direct variation with the growth of S_c. But, for inverse variation, though the concentration enhances initially with the rise of S_c but gradually it diminishes as shown in fig. 4.13. Schmidt number is the proportion of momentum and mass diffusivity means diffusion coefficient is inversely proportional to Schmidt number and hence due to increasing values of Schmidth number (S_c), the diffusion coefficient is diminished, which reduces the solute boundary layer thickness for direct and inverse variations after crossing the certain distance in the plate.

The variation of first order chemical reaction rate parameter (β) for the concentration curves $\phi(\eta)$ against η are depicted in figs. 4.14 and 4.15 for direct and inverse variations. The smoothness of the curves is observed in the direct variation which indicates that the reaction rate parameter is highly constructive and hence constructive chemical reaction is possible. But, for inverse variation, uneven or bumpy curves are seen which implies that

the reaction rate parameter is highly destructive. Therefore, mass transport from the plate occurs in a destructive reaction, while mass absorption takes place in a constructive reaction. Also, the thickness of solute boundary layer diminishes as β rises.

Figs. 4.16 and 4.17 demonstrate the impact of varying surface concentration on the concentration profile for distinct positive and negative values of n. As n value increases for direct variation, it is noticeable from fig. 4.16 that the concentration curves $\phi(\eta)$ and the thickness of solute boundary layer diminish. For inverse variation, however, the surface concentration diminishes as n reduces, as shown in fig. 4.17. Also, mass absorption is noticed in inverse variation, and as the value of $n\ (< 0)$ rises, mass absorption enhances.

Skin friction calculation is essential for engineers to determine the total frictional drag exerted on the object and to estimate the heat transport rate on its surface. The skin friction coefficient τ is plotted in fig. 4.18 against applied suction for rising values of elastico-viscous parameter. It shows that the viscous drag though initially enhances but gradually reduces with growing elastico-viscous parameter. The growing applied suction factor diminishes the coefficient of skin friction at a certain length of the plate and then it enhances along with the plate.

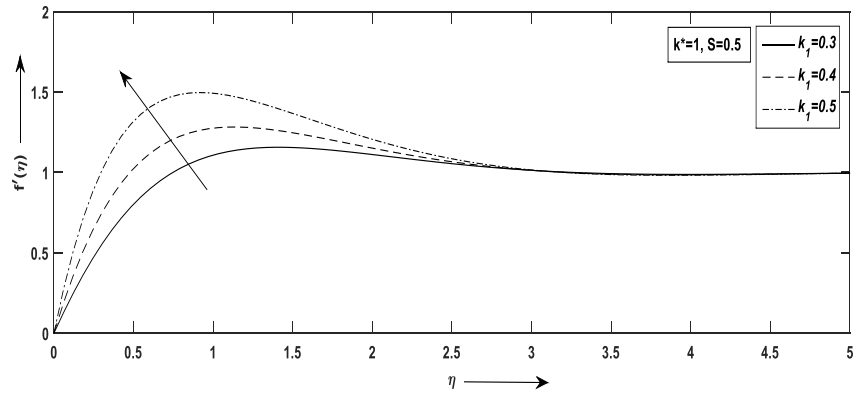

Fig. 4.2 $f'(\eta)$ versus η with variation of k_1

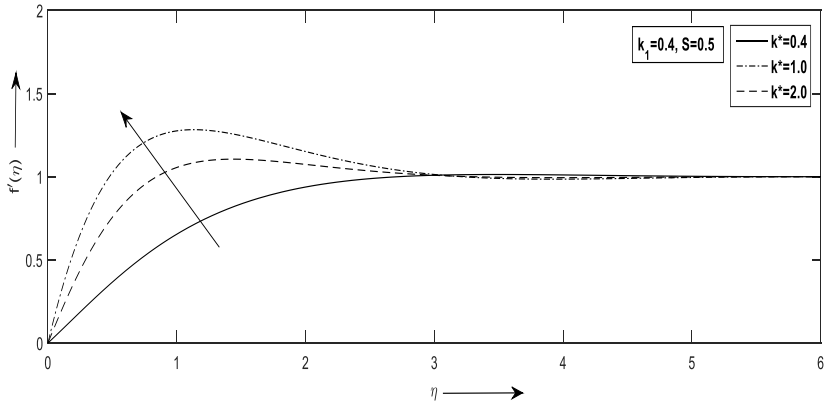

Fig 4.3 $f'(\eta)$ versus η with variation of k*

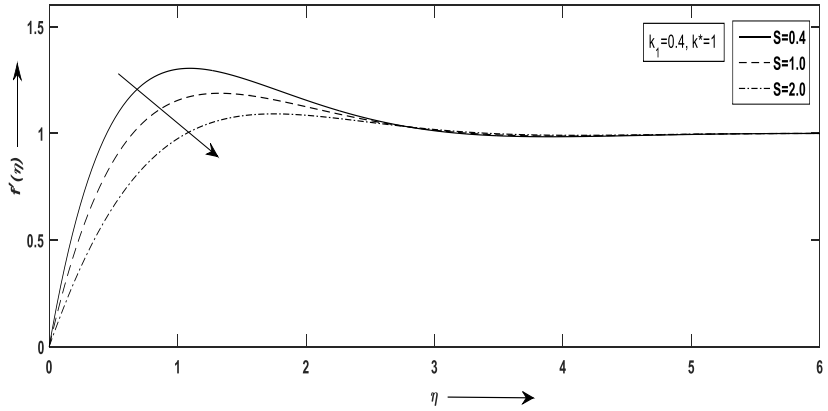

Fig. 4.4 $f'(\eta)$ versus η with variation of suction S

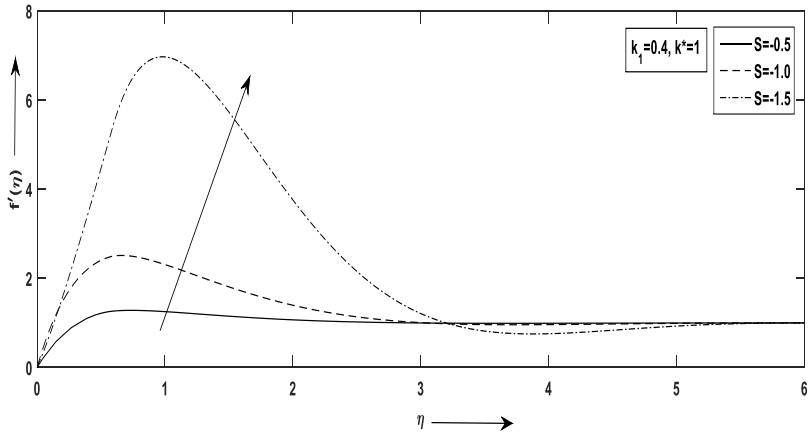

Fig. 4.5 $f'(\eta)$ versus η with variation of blowing S

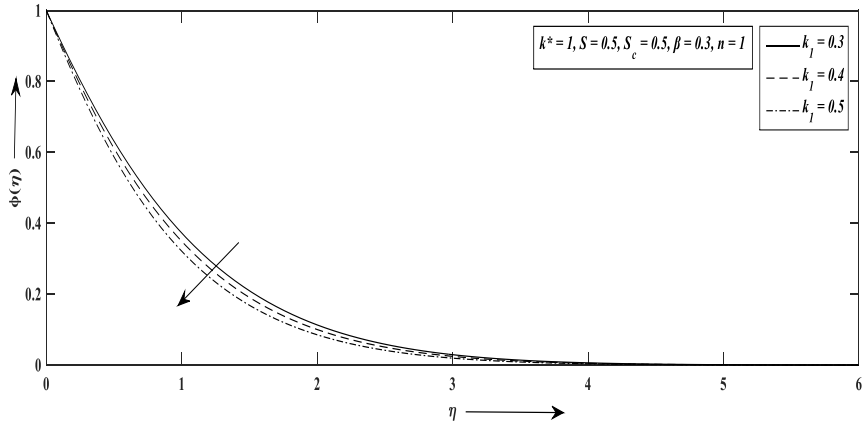

Fig. 4.6 $\phi(\eta)$ versus η for variation of k_1 for n > 0

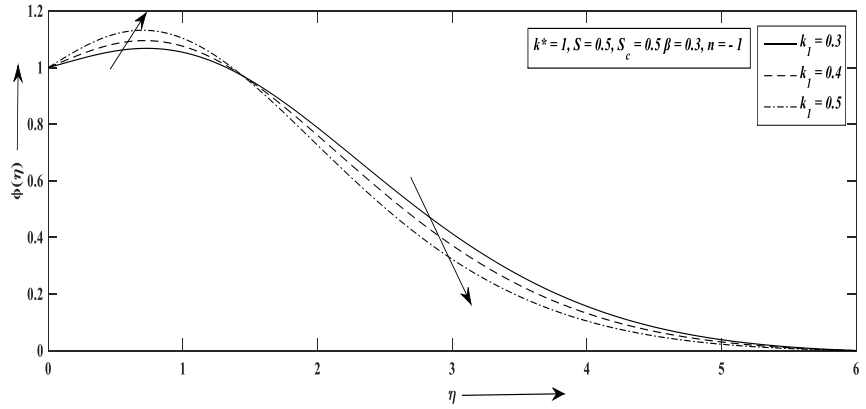

Fig. 4.7 $\phi(\eta)$ versus η for variation of k_1 for n < 0

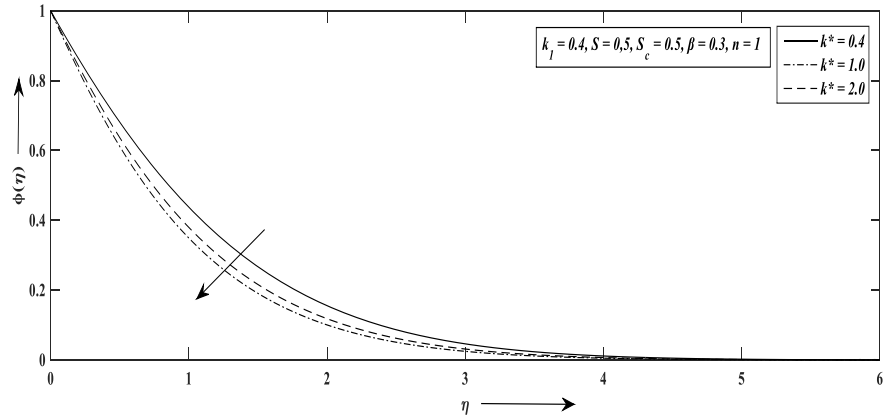

Fig. 4.8 $\phi(\eta)$ versus η for variation of k* for n > 0

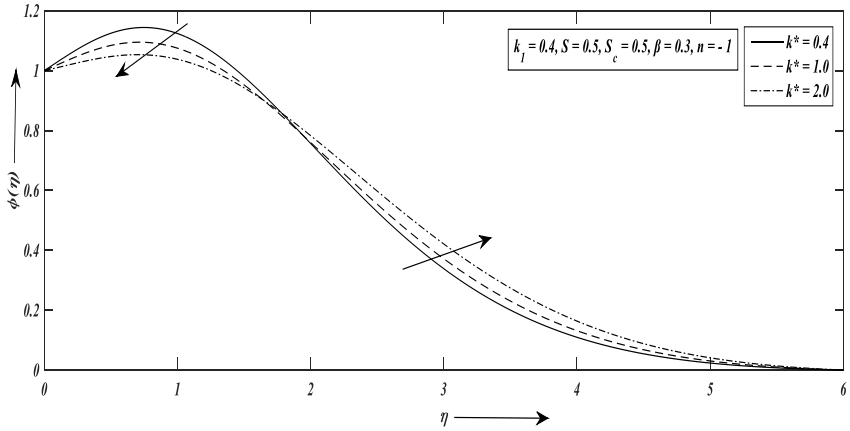

Fig. 4.9 $\phi(\eta)$ versus η for variation k* for n < 0

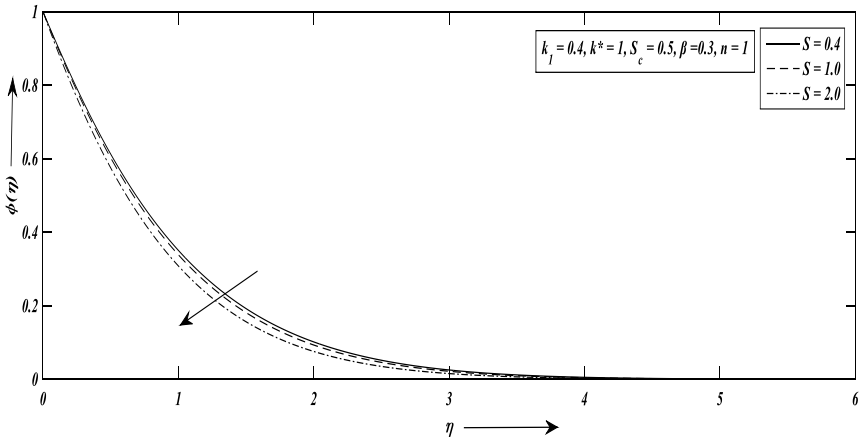

Fig. 4.10 $\phi(\eta)$ versus η for variation of S for n > 0

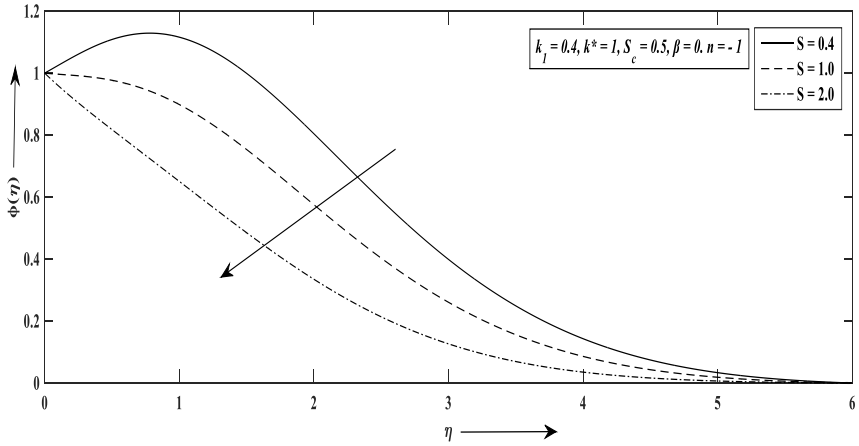

Fig. 4.11 $\phi(\eta)$ versus η for variation of S for n < 0

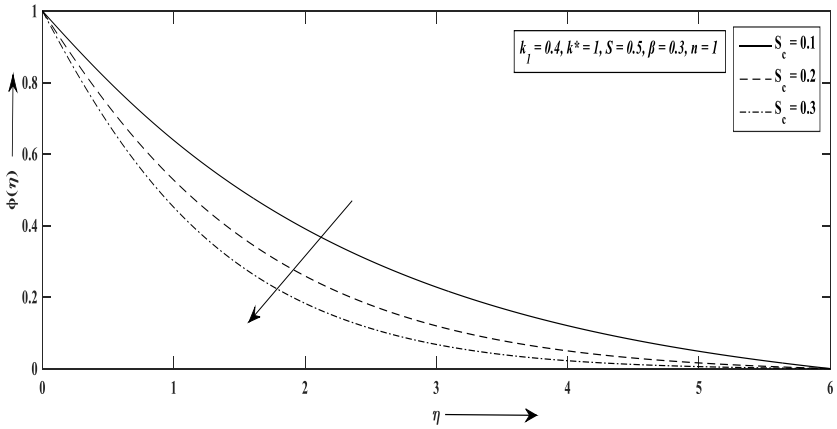

Fig. 4.12 $\phi(\eta)$ versus η for variation of S_c for n > 0

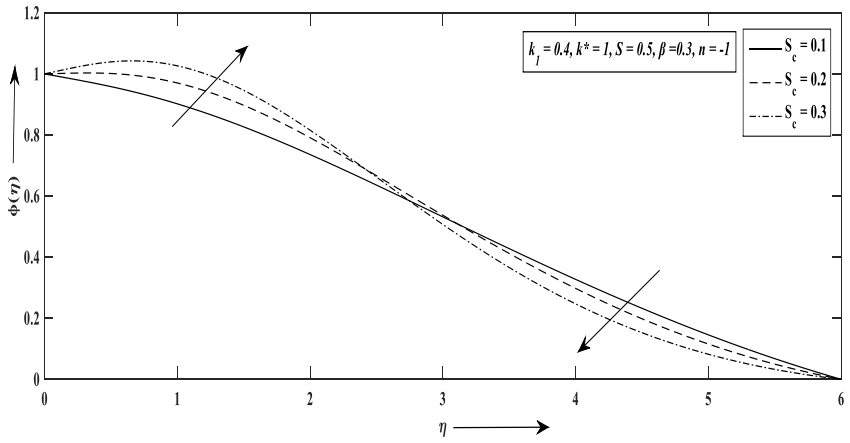

Fig. 4.13 $\phi(\eta)$ versus η for variation of S_c for n < 0

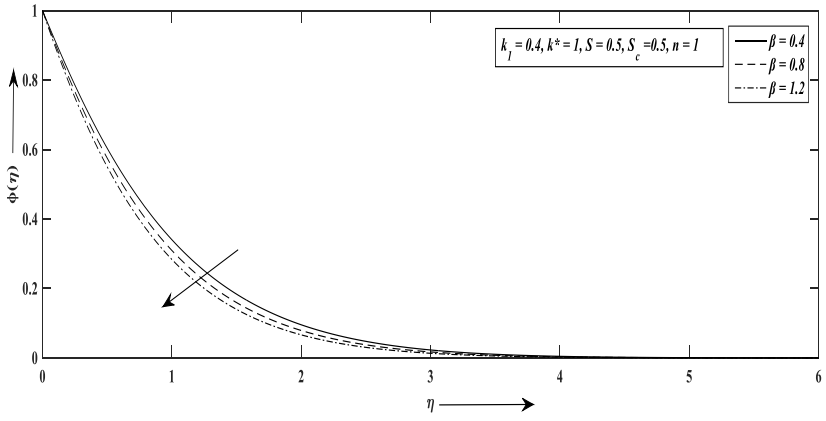

Fig. 4.14 $\phi(\eta)$ versus η for variation of β for n > 0

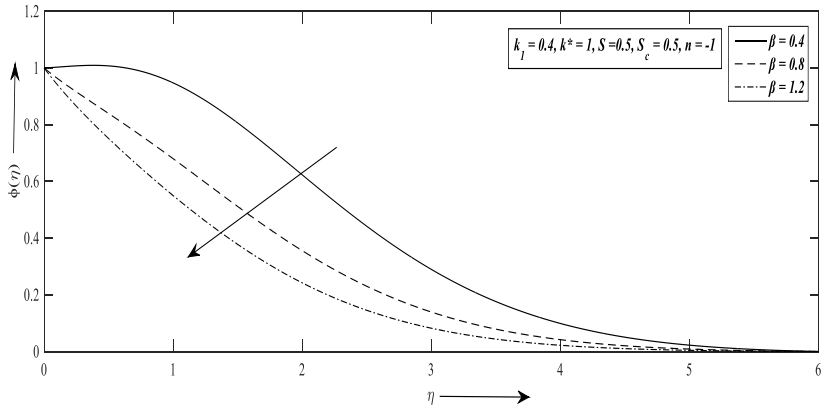

Fig. 4.15 $\phi(\eta)$ versus η for variation of β for n < 0

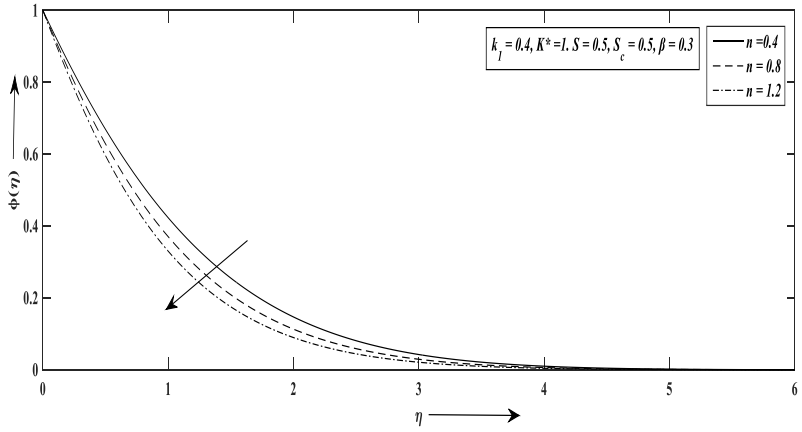

Fig. 4.16 $\phi(\eta)$ versus η for variation of n > 0

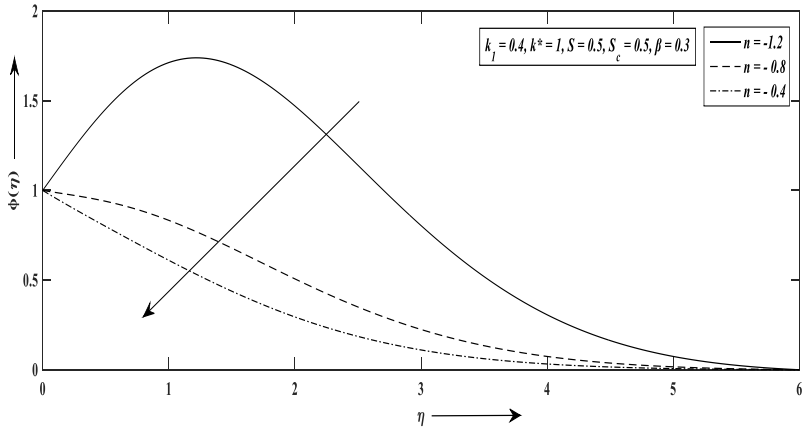

Fig. 4.17 $\phi(\eta)$ versus η for variation of n < 0

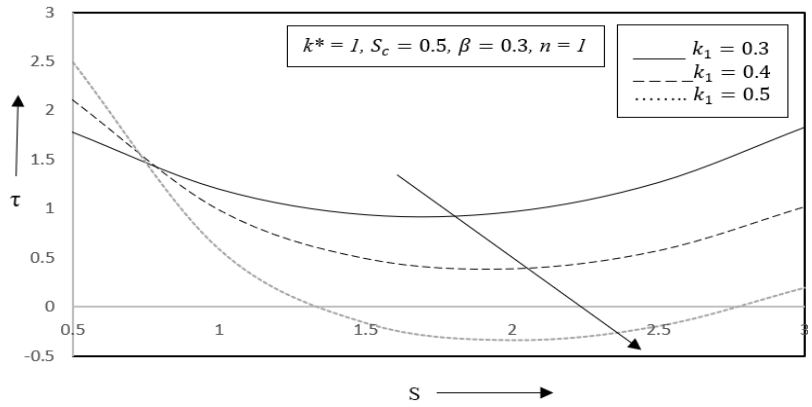

Fig. 4.18 τ versus S for variation of k_1

4.5 Conclusion

The study reveals that the growth of elastico-viscosity and permeability enhances fluid motion but it reduces the concentration of the fluid for direct variation. For inverse variation, though the concentration rises at the leading age of the plate but gradually it starts decreasing with the growing elastico-viscosity and permeability factors. The velocity and concentration for direct and inverse variation also diminish as the suction parameter enhances. The concentration reduces with the rise of Schmidt number for direct variation but for inverse variation initially, it rises but ultimately it reduces. For both direct and inverse variation, the reaction rate parameter lowers the fluid concentration. The increasing positive values of surface concentration reduces the concentration smoothly but the negative values of surface concentration diminish the concentration abruptly. The drag force reduces with the growth of suction. This work can be extended due to its numerous applications. Various analytical and numerical techniques can be utilized for comparing the present findings. The fluid flow simulation can be used to get a clear image of the generated outcomes.